(34) Matsuo, M.; Manley, R. S. J. *Macromolecules* **1982**, *15*, 985.
(35) Smith, P.; Lemstra, P. J.; Pijpers, J. P. L.; Kiel, A. M. *Colloid Polym. Sci.* **1981**, *259*, 1070.
(36) Bunn, C. W.; de Daubeny, R. *Trans. Faraday Soc.* **1954**, *50*, 1173.
(37) Cannon, C. G. *Polymer* **1982**, *23*(8), 1123.
(38) Read, B. E.; Stein, R. S. *Macromolecules* **1968**, *1*, 116.
(39) Cembrola, R. J.; Kyu, T.; Stein, R. S.; Suehiro, S.; Kawai, H. *J. Polym. Sci., Polym. Phys. Ed.* **1983**, *21*, 881.
(40) Roy, S. K. Ph.D. Thesis, McGill University, Montreal, Canada, 1986.
(41) Smith, P.; Lemstra, P. J. *J. Mater. Sci.* **1980**, *15*, 505.
(42) Anandakumaran, K.; Roy, S. K.; Manley, R. S. J. *Macromolecules*, following paper in this issue.
(43) Takayanagi, M.; Matsuo, T. *J. Macromol. Sci. Phys.* **1967**, *B1*, 407.
(44) Takayanagi, M. *Mem. Fac. Eng., Kyushu Univ.* **1963**, *23*(1), 1.
(45) Kyu, T. Ph.D. Thesis, Kyoto University, Kyoto, Japan, 1980.

Drawing-Induced Changes in the Properties of Polyethylene Fibers Prepared by Gelation/Crystallization

K. Anandakumaran, S. K. Roy, and R. St. John Manley*

Pulp and Paper Research Institute of Canada and Department of Chemistry, McGill University, Montreal, Quebec, Canada H3A 2A7. *Received April 30, 1987; Revised Manuscript Received December 8, 1987*

ABSTRACT: Fibers of ultrahigh molecular weight polyethylene were prepared by drawing dry specimens obtained by gelation/crystallization from solution. The maximum draw ratio (λ) attained was 250. The properties of the fibers were assessed by measurements of density, birefringence, differential scanning calorimetry, infrared dichroism, sonic velocity, and dynamic modulus. The results have been analyzed in terms of a two-phase model of crystalline and amorphous regions. All properties approach a limiting value at a draw ratio of about 100. The degree of crystallinity and melting point decrease initially (for $\lambda < 12$) and then increase rapidly with λ up to their limiting values. The crystalline orientation function, as determined from measurements of infrared dichroism, increases rapidly with λ and reaches its maximum value at $\lambda \simeq 10$. In contrast, the amorphous orientation function, as estimated from sonic velocity and birefringence measurements, increases almost linearly and reaches its maximum value at $\lambda \simeq 100$. The increase in modulus with draw ratio correlates with the amorphous orientation function but not with the orientation of the crystalline phase. On the basis of the various observations, the sequence of events during drawing is discussed.

Introduction

In recent years the processing of high molecular weight polyethylene to give fibers with high stiffness and strength has attracted considerable interest. The basic prerequisite for achieving this objective is that the chain molecules should be fully extended and aligned in the draw direction. For this purpose Smith and Lemstra[1,2] have introduced the technique of gelation/crystallization. In this process a thermoreversible gel is formed by rapidly quenching a hot dilute solution of the polymer. In the three-dimensional network thus formed the crystalline regions act as junction points.[3] The gels exhibit very high extensibility, even after removal of the solvent, and this is attributed to the significantly reduced chain entanglement density in comparison with melt-crystallized material.[1]

The structure and properties of drawn gelation-crystallized specimens have been extensively studied, especially for the range of draw ratios below 100, but the details of the deformation process are not fully understood. In particular there is the question as to whether the properties increase linearly up to the highest attainable draw ratios or approach a limiting value. Secondly since, as will be seen later, gelation-crystallized specimens are essentially a two-phase system, it is of interest to ascertain the effect of draw ratio on the molecular orientation of the crystalline and amorphous phases. The present work attempts to address these issues by a quantitative study of the uniaxial deformation process in dry ultrahigh molecular weight polyethylene gelation/crystallized samples. Toward this end changes in the properties of the uniaxially deformed films with increasing draw ratio have been assessed by measurements of birefringence, density, differential scanning calorimetry, infrared dichroism, sonic velocity, and dynamic modulus. The results allow characterization of the deformation mechanism that is involved.

Experimental Section

Specimen Preparation. The sample used was linear polyethylene (Hercules 1900/90189) with a nominal intrinsic viscosity of 30 dL/g, corresponding to a molecular weight of 6×10^6. The solvent was decalin.

Gel films were prepared by crystallization from solution. The decalin solution at a concentration of 0.4 g/dL, containing 0.1% w/w of the antioxidant di-*tert*-butyl-*p*-cresol, was prepared by heating the polymer/solvent mixture at 150 °C for about 1 h under nitrogen. The hot solution was quenched by pouring into an aluminum tray surrounded by ice water, thus generating a gel. The decalin was allowed to evaporate from the gel in a current of air under ambient conditions. Residual solvent in the film thus obtained was removed by extraction with ethanol, and after air-drying the thickness of the film was about 300 μm.

Rectangular shaped samples with dimensions of 50×10 mm were cut from the film and drawn on an Instron tensile testing machine fitted with a temperature-regulated oven. The samples were drawn at a cross head speed of 10 mm/min at a temperature of 130–135 °C. The draw ratio (λ) was determined in the usual way by measuring the displacement of ink marks placed on the sample surface prior to drawing at intervals of 2 mm.

Density. Densities (ρ) of the various samples were measured in an 2-propanol–water density gradient column calibrated with glass beads of known density. From the measured densities (ρ), the weight fraction of crystalline material W_c was calculated from eq 1 where ρ_c is the density of the crystalline material, taken as

$$W_c = \frac{\rho_c (\rho - \rho_a)}{\rho (\rho_c - \rho_a)} \quad (1)$$

0.997 g/cm^3, and ρ_a, the density of the amorphous phase, was assumed to be 0.854 g/cm^3.[4]

For oriented samples it was necessary to remove air bubbles, by pressing at 3000 psi (2×10^7 Pa) at room temperature, prior to the flotation measurements.

0024-9297/88/2221-1746$01.50/0

Thermal Measurements. Melting endotherm curves were recorded with a Perkin-Elmer differential scanning calorimeter Model DSC-2C. Samples of about 2 mg were heated at a constant rate of 10 °C/min, using standard aluminum sample pans that were sealed. Indium was used as a standard for the instrument calibration. The weight fraction of crystalline material was calculated from the relation (2), where ΔH is the heat of fusion

$$W_c = \Delta H/\Delta H^\circ \quad (2)$$

of the sample and ΔH° is that of a perfect orthorhombic polyethylene crystal; the value of ΔH° was taken as 69 cal/g (289 J/g).[4] In these calculations it was assumed that for any other phases present (e.g., triclinic) the heat of fusion is equal to that of the orthorhombic form. Melting points were determined from the position of the maximum in the fusion curves.

Birefringence. The birefringence of oriented samples was measured by using a Ehringhaus quartz rotary compensator with a Reichert Zetopan-Pol polarizing microscope and a green line (λ = 546 nm) interference filter.

The birefringence was calculated from the relation (3),[5] where

$$\Delta n_T = \Gamma_\lambda/t \quad (3)$$

Δn_T is the total birefringence of the specimen, Γ_λ is the measured retardation at a specified wavelength λ, and t is the specimen thickness measured with a micrometer or by dividing the weight of a rectangular piece of sample by the product of its density and area.

Sonic Velocity. The sonic velocity in the specimens was determined by measuring the transit time of a sound pulse between two transducers coupled to the specimens. The measurements were made by using a Dynamic Modulus tester (Model ppm-5) at a frequency of 5 kHz. For oriented samples, specimens of dimensions 10–15 cm × 0.3 cm were used, while for unoriented samples the dimensions were 8–10 cm × 0.6 cm. From the known sonic velocity and specimen density the sonic modulus (Young's modulus) is given by the relation (4),[5,6] where E is the sonic modulus, ρ is the density, and C is the sonic velocity.

$$E = \rho C^2 \quad (4)$$

Infrared Absorption Measurements. The infrared absorption measurements were made with a Nicolet 6000 FTIR spectrometer. The specimens were placed at 45° in the clockwise direction from the slit. The gold wire grid polarizer was then set at the 45° position to measure the absorption ($A_\parallel$) in the direction parallel to the fiber axis (draw direction) and at the 315° position to obtain the absorption ($A_\perp$) in the direction perpendicular to fiber axis. From the measured absorption the dichroic ratio (D) is obtained as[7]

$$D = A_\parallel/A_\perp \quad (5)$$

It is well-known that for polyethylene the 730 cm^{-1} band absorbs only in the crystalline region. It is also known[8] that the 720 cm^{-1} band is due mainly to the crystalline regions although there may be some contribution from the amorphous regions. Therefore, the dichroic ratios were measured at these two frequencies, and, as will be seen later, these values were used to estimate the crystalline orientation functions.

Dynamic Storage Moduli. Dynamic storage moduli were measured with a Rheovibron (Model DDV-IIC) viscoelastometer at 110 Hz and room temperature. Sample lengths were typically 5 cm.

Results and Discussion

Degree of Crystallinity and Fusion Behavior. In discussing the drawing behavior of the polyethylene gel films it seems important to focus first on the structure of the initial undrawn isotropic specimens. In earlier work it was shown that dry gel films, prepared in the manner described above, are similar to single crystal mats[9] in which the lamellae are predominantly parallel to the plane of the film which is also the draw direction. Presumably coherence between the individual lamellar crystals is provided by trapped molecular entanglements.

Accordingly, the drawing starts from an initial structure in which the chains are oriented perpendicular to the draw direction. Such a film constitutes a two-phase system of crystalline and amorphous regions. The amorphous regions are associated with the interfacial zones of the crystals where the folds are localized, as well as with topological defects (entanglements) in the interlamellar regions. The crystalline regions correspond to the core of the lamellae. In what follows, the results will be interpreted in terms of this two-phase system of crystalline and noncrystalline regions, while recognizing that the intrinsic properties of the two phases may change with orientation and morphology, as demonstrated by Adams et al.[10] and by Wedgewood and Seferis.[11]

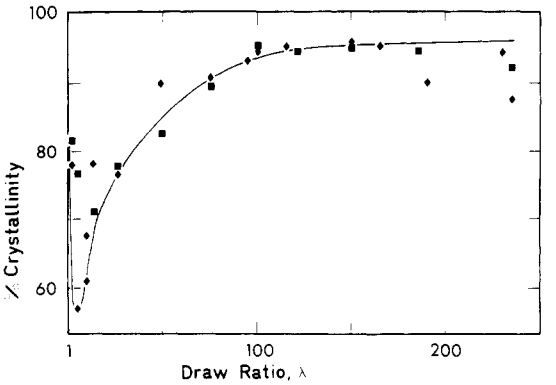

Figure 1. Crystallinity of dry gelation-crystallized ultrahigh molecular weight polyethylene specimens as a function of draw ratio: (♦) DSC; (■) density.

Figure 1 shows the crystallinity of the samples as obtained from density and heat of fusion measurements. The variation of the crystallinity with draw ratio appears to occur in three stages. First, there is an initial decrease in crystallinity for $\lambda < 12$; this is followed by a rapid increase up to a crystallinity of about 95% which is attained at a draw ratio of about 100. For still higher draw ratios the crystallinity seems to remain essentially constant, although at the highest draw ratios there is some indication of a slight decrease. The initial decrease in crystallinity at low draw ratios is not unexpected: a similar effect has been observed by Glenz and Peterlin[12] for drawn samples of melt crystallized material, by Smook and Pennings[13] for hot drawn gel-spun fibers, and by Porter et al.[14] for solid-state extrusion of high-density polyethylene. The subsequent increase in crystallinity up to the plateau can probably be attributed to a decrease in the number of entanglements and the removal of the folds during the transformation from the initial lamellar structure to an extended-chain configuration in the fully drawn fiber. The maximum level of crystallinity (95%) that is finally attained beyond λ = 100 suggests that even in the fully drawn fiber there is some deficiency in the perfection of the extended-chain crystals that are formed. The structure of the highly drawn fibers can thus be envisaged as more or less continuous, with various defects (e.g., chain ends and kinks) randomly distributed in them.

In the assessment of crystallinity from the density measurements, it has been tacitly assumed that the density of the crystalline and amorphous phases remains constant during extension. However, for solid-state extruded polyethylene Adams et al.[10] have shown that as the draw ratio increases the amorphous density increases and the crystal density decreases. These effects are expected to lead to errors in assigning the degree of crystallinity, especially in high crystallinity samples. Using the data of Adams et al.,[10] we have estimated that the crystallinity of our most highly drawn samples could be in error by a maximum of about 4%.

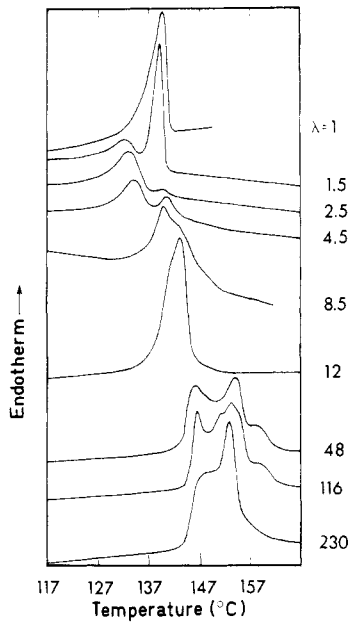

Figure 2. Selected DSC curves for dry gelation-crystallized UHMW polyethylene samples at various draw ratios: scan speed, 10 °C/min.

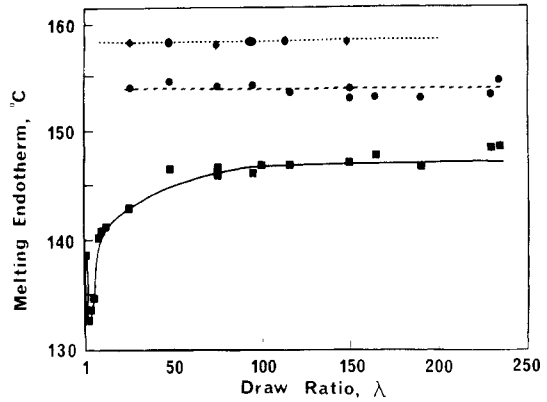

Figure 3. Peak melting temperatures of dry gelation-crystallized ultra-high molecular weight polyethylene specimens as a function of draw ratio.

Figure 2 shows selected DSC curves recorded at a scan speed of 10 °C/min for samples drawn to various draw ratios. For the original undrawn sample a single endotherm is observed. At low draw ratios ($\lambda < 12$) there are two peaks, and at still higher draw ratios three melting peaks are observed, although as mentioned by Miyasaka et al.[15] the highest melting peak was generally not well-defined for the most highly drawn samples ($\lambda > 200$). The peak melting temperatures are plotted against draw ratio in Figure 3. In this figure the second (higher temperature) peak for samples with $\lambda < 12$ has been omitted because its origin is not understood at present. For the first (lowest temperature) peak the melting temperature showed an initial decrease from 138 °C at $\lambda = 1$ to 133 °C at $\lambda \simeq 5$; at higher draw ratios the melting temperature increases with λ and attains a plateau value of T_m = 145 °C for values of $\lambda > 100$ corresponding to a fully drawn fiber. Since the value of T_m in the plateau region corresponds to the reported[16] equilibrium melting temperature of orthorhombic polyethylene, the low temperature peak can be assigned to the normal melting of crystalline polyethylene. For the second peak, which occurs in specimens with $\lambda > 25$, the melting temperature remained constant at about 154 °C over the entire range of draw ratios. This peak has been assigned to a solid-solid transformation from

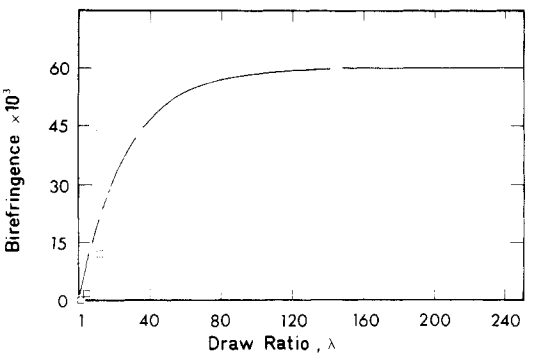

Figure 4. Birefringence of dry UHMW gelation-crystallized polyethylene samples as a function of draw ratio. The solid line was obtained by fitting the data points with the exponential function $y = 60\,(1 - e^{-0.0377x})$ where y = birefringence and x = draw ratio.

the orthorhombic to a hexagonal phase in the constrained parts of the sample during heating.[17] The temperature corresponding to the third (highest temperature, T_m = 158 °C) peak in specimens with $\lambda > 25$ remains constant with draw ratio over the range where it could be observed. This endotherm has also been previously observed in drawn melt-crystallized polyethylene[18] and in surface grown fibers;[17] it is thought to be due to the melting of the hexagonal phase, but there is reason to believe that this interpretation may be an oversimplification.[15] For present purposes the most striking feature of the melting behavior is the variation of the melting temperature of the first (low temperature) peak with draw ratio. The initial decrease and subsequent increase up to a plateau with increasing draw ratio is analogous to and consistent with the variation of crystallinity with draw ratio (Figure 1). Since the melting temperature of a crystal is an index of the lattice perfection, it seems reasonable to suppose that the initial decrease in the melting point and crystallinity at low draw ratios is due to the destruction of the crystalline lamellae, as a result of plastic deformation, leading to small blocks of folded chains, presumably held together by tie molecules.

Birefringence. Birefringence was not detectable in the original unoriented sample. Figure 4 shows the birefringence of the polyethylene fibers at various draw ratios. The solid line was obtained by fitting the data with an exponential function. Apparently the variation of birefringence with draw ratio occurs in two stages. The birefringence increases rapidly with increasing λ and approaches a plateau value of about 61×10^{-3} for draw ratios higher than $\lambda = 100$. The intrinsic birefringence of a perfect extended-chain paraffin ($C_{36}H_{74}$) crystal is 58.3×10^{-3}.[19] Thus in the plateau region beyond $\lambda = 100$ the crystal c axis is oriented parallel to the draw direction. This means that the orientation process is to all intents and purposes complete at the onset of the plateau region. Further deformation can presumably only occur by chain slippage. These birefringence results are consistent with findings of other investigations.[20,21]

Degree of Crystalline and Amorphous Orientation. As discussed earlier the gelation-crystallized samples of polyethylene are essentially a two-phase system. During the deformation process rearrangements occur in both the crystalline and amorphous regions. Thus in order to understand the drawing process, it is important to have a knowledge of the changes in orientation in both regions as the draw ratio increases. In the present work the degree of molecular orientation in the crystalline regions was characterized by the crystalline orientation function derived from measurements of the infrared dichroic ratios

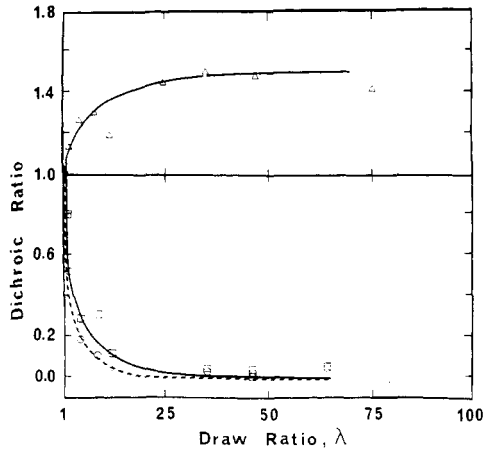

Figure 5. Infrared dichroic ratio versus draw ratio for the crystalline (□, 720, ○, 730 cm^{-1}) and amorphous bands (△, 1368 cm^{-1}) of dry gelation-crystallized UHMW polyethylene specimens.

of the drawn samples. The orientation of the amorphous phase with draw ratio was determined from sonic velocity and birefringence measurements.

Considering first the infrared measurements, it is generally agreed that the 720 and 730 cm^{-1} bands are due to absorption by the crystalline phase only and have been assigned as due to a CH_2 rocking mode of the chain, the 720 cm^{-1} component having a transition moment along the *b* axis and the 730 cm^{-1} component being polarized along the *a* axis.[7] There is also agreement[12] that the 1368 cm^{-1} band is due exclusively to absorption by the amorphous phase and has been assigned as due to a CH_2 wagging mode where CH_2 groups are in a gtg or gtg′ conformation.

The infrared dichroic ratios of the oriented gelation-crystallized samples are given in Figure 5. The dichroic ratios corresponding to the amorphous band (1368 cm^{-1}) increase with draw ratio and appear to level off beyond $\lambda = 15$. This effect is primarily due to the orientation of trans units that are flanked by gauche units and cannot be specifically related to the amorphous chain orientation due to the limitation of obtaining the transition moment angle with respect to *c* axis.[12] It may be noted that for samples drawn beyond $\lambda = 75$ the amorphous band (1368 cm^{-1}) disappeared completely from the absorption spectrum, corresponding to the diminished level of the gtg triads. The dichroic ratios corresponding to the crystalline bands decrease with draw ratio and level off beyond $\lambda \simeq 25$. The present results are in agreement with literature data[22] and indicate that the *a* axis orients more readily than the *b* axis.

From the measured dichroic ratios for the crystalline bands D_{730} and D_{720} the orientation function for the polyethylene crystal *a* and *b* axis, f_a and f_b, were derived[8] from eq 6 and 7.

$$f_a = \frac{D_{730} - 1}{D_{730} + 2} \tag{6}$$

$$f_b = \frac{D_{720} - 1}{D_{720} + 2} \tag{7}$$

For orthorhomic polyethylene where the *a*, *b*, and *c* axes are mutually perpendicular, the orientation functions of the three crystal axes are related by eq 8.

$$f_a + f_b + f_c = 0 \tag{8}$$

Thus knowing f_a and f_b the orientation function of the crystal *c* axis could be determined. The results are given by the dashed line in Figure 6.

The orientation function f_c of perfectly oriented chains

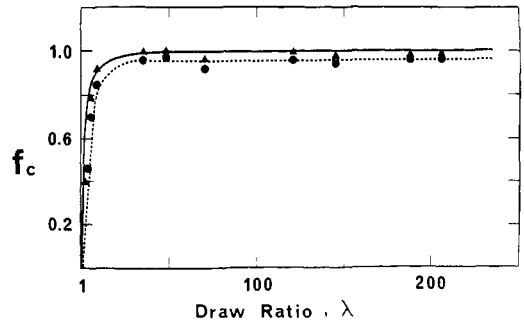

Figure 6. Crystalline orientation function (f_c) versus draw ratio for dry gelation-crystallized specimens of UHMW polyethylene: (●) from eq 8; (▲) from eq 9.

relative to the draw direction can also be obtained from the Hermans orientation function which is related to the dichroic ratio of the crystalline bands by eq 9, where D_0,

$$f_c = \frac{(D - 1)(D_0 + 2)}{(D + 2)(D_0 - 1)} \tag{9}$$

the dichroic ratio of an ideally oriented sample, is given by $D_0 = 2 \cot^2 \phi$, and ϕ is the transition moment angle between the molecular chain axis and the infrared transition moment. For polyethylene the transition moment angle $\phi = 83°$ for the 730 cm^{-1} crystalline band.[5] The Hermans orientation function f_c obtained by using the dichroic ratios corresponding to the 730 cm^{-1} crystalline band was calculated from eq 9. The results as a function of draw ratio are shown by the solid line in Figure 6. It is seen that the data for the two methods employed (eq 8 and 9) are in essential agreement; the values of f_c increase rapidly with draw ratio and attain a value corresponding to maximum orientation ($f_c = 1$) at $\lambda \simeq 10$. It should be noted, however, that the Hermans orientation function is not a good measure of orientation for highly oriented systems. Its variation is insensitive to variation of the orientation angle about zero. Therefore the fact that $f_c \simeq 1$ does not necessarily imply that molecular rearrangements have ceased. Small changes, such as the unfolding of the last loops or kinks, which cannot be sensed by measurements of the orientation function, may still occur.

We turn not to the variation of the amorphous orientation function with draw ratio. Samuels[5,6] has shown that for an unoriented sample the relation between the measured sonic modulus E_u and the fraction of crystalline (β) and amorphous ($1 - \beta$) phases present is

$$\frac{3}{2E_u} = \beta/E^\circ_{t,c} + (1 - \beta)/E^\circ_{t,am} \tag{10}$$

where $E^\circ_{t,c}$ is the intrinsic modulus of the crystalline regions and $E^\circ_{t,am}$ is the intrinsic modulus of the amorphous regions. In order to use eq 10 sonic modulus and density measurements were made on unoriented samples of Marlex 6009 and UHMW polyethylene crystallized from melt under various conditions. By plotting $3/2E_u\beta$ against $(1 - \beta)/\beta$, a linear relation was obtained in accordance with eq 10 (see Figure 7) and values of the constants $E^\circ_{t,am}$ and $E^\circ_{t,c}$ (as obtained from the slope and intercept) were 0.524×10^{10} and 4.76×10^{10} dyn/cm^2, respectively. These values are in good agreement with those obtained by other investigators for polyethylene.[23]

For an oriented sample the sonic modulus equation is

$$\frac{3}{2}(\Delta E^{-1}) = \frac{\beta f_c}{E^\circ_{t,c}} + \frac{(1 - \beta) f_{am}}{E^\circ_{t,am}} \tag{11}$$

where $(\Delta E^{-1}) = (\Delta E_u^{-1} - E_{or}^{-1})$, E_{or} is the measured sonic modulus of the oriented sample, and f_c and f_{am} are the orientation functions of the crystalline and amorphous

Table I
Experimental Data Used in Equations 11 and 12 for Calculating f_{am}

λ	density, g/cm³	β crystalline fractn	f_c from eq 9	birefringence,[a] $\Delta n_T \times 10^3$	sonic modulus, GPa	f_{am} from sonic modulus	f_{am} from birefringence
1	0.9680	0.821			4.55		
12	0.9500	0.705	0.852	21.83	11.9	0.138	
35	0.9615	0.780	0.995	43.96	54.3	0.330	
48	0.9680	0.821	1.00	49.41	62.9	0.390	0.120
70	0.9795	0.893	0.959	55.71	100	0.660	0.540
120	0.9874	0.942	0.998	59.35	101	1.04	0.827
145	0.9873	0.940	0.980	59.75	116	1.07	1.00
185	0.9870	0.940	0.994	59.97	130	1.05	0.932

[a] Obtained from the solid line in Figure 4.

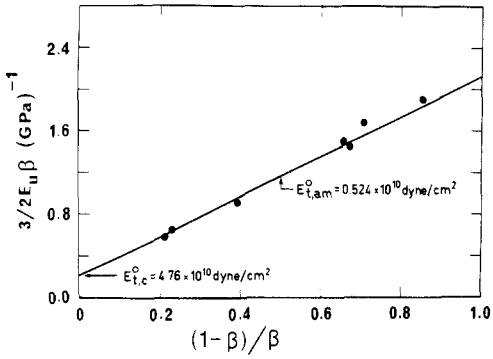

Figure 7. Determination of the intrinsic moduli of the crystalline and amorphous regions of polyethylene.

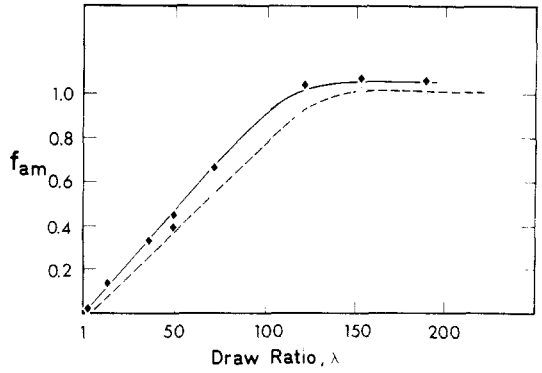

Figure 8. Amorphous orientation function (f_{am}) versus draw ratio for dry gelation-crystallized specimens of UHMW polyethylene: (♦) sonic velocity; (◇) birefringence.

regions, respectively. Thus the values of f_{am} for the oriented gelation-crystallized samples were calculated from eq 11 by using the measured values of E_{or}, β, and f_c together with the constants $E^\circ_{t,c}$ and $E^\circ_{t,am}$ derived from the unoriented samples. The results are shown in Table I and Figure 8.

The amorphous orientation function can also be obtained from the birefringence data. The birefringence equation for a uniaxially oriented system can be written in the form

$$\Delta n_T = \Delta n^\circ_c f_c \beta + \Delta n^\circ_{am} f_{am}(1 - \beta) + \Delta n_f \qquad (12)$$

where Δn_T is the measured birefringence, Δn_f is the form birefringence which is usually assumed to be negligible,[24,25] Δn°_c and Δn°_{am} are the intrinsic birefringence of the crystalline and amorphous phases, respectively, and the other symbols have the same meaning as previously defined. For linear polyethylene Wedgewood and Seferis[11] have shown that the intrinsic birefringence of the crystalline and amorphous phases are $\Delta n^\circ_c = 0.0585$ and $\Delta n^\circ_{am} = 0.194$ for samples exhibiting spherulitic morphology, while for samples with a fibrillar morphology $\Delta n^\circ_c = 0.0585$ and $\Delta n^\circ_{am} = 0.12$. Thus the intrinsic birefringence of the amorphous

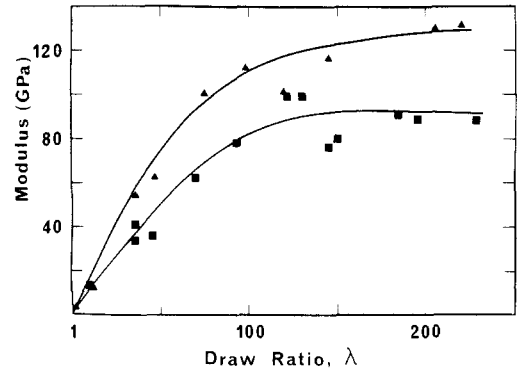

Figure 9. Sonic modulus and dynamic storage modulus as a function of draw ratio for dry gelation-crystallized specimens of UHMW polyethylene: (■) dynamic modulus; (▲) sonic modulus.

phase changes with orientation and morphology. As shown by WAXD studies[26] the specimens used in the present work are clearly fibrous; therefore it is appropriate to take $\Delta n^\circ_{am} = 0.12$, as proposed by Wedgewood and Seferis.[11] For the crystalline phase we have taken $\Delta n^\circ_c = 0.057$, since this is the value most frequently encountered in the literature.[24,25,27] Using these values of the intrinsic birefringences together with the measured values of Δn_T, f_c, and β, values of f_{am} were estimated from eq 12. The results are shown in Table I and Figure 8 as a function of draw ratio. It may be noted that for samples in the range of $\lambda < 50$ the calculated values of f_{am} are negative and thus are not shown in the figure. This effect is probably due to inaccuracies of the measured birefringences.

It can be readily seen that the trend in f_{am} from the birefringence and sonic velocity measurements is consistent. Comparing Figure 6 and 8, it is seen that the crystallite orientation f_c increases rapidly and reaches a maximum at low draw ratios ($\lambda \sim 10$), while the amorphous orientation f_{am} increases almost linearly below $\lambda = 100$ and reaches a limiting value at higher draw ratios. Thus molecular rearrangements occur more rapidly in the crystalline regions than in the amorphous phase.

It is interesting to note that the rapid increase in f_c evidenced in Figure 6 occurs in the same range of λ where the degree of crystallinity and melting point show an initial decrease. It thus seems reasonable to suppose that these two effects are related. The likely explanation is that at low draw ratios the original lamellae break up into crystallite blocks which rapidly reorient with their c axes in the draw direction, a process that is accompanied by a decrease in crystallinity and melting point.

Mechanical Measurements. Figure 9 shows a plot of the sonic (Young's) modulus and the dynamic storage modulus against draw ratio. Initially the moduli increase rapidly and then approach a limiting value for draw ratios greater than $\lambda \simeq 100$. This behavior is fully consistent with trends observed in the other properties. It should be

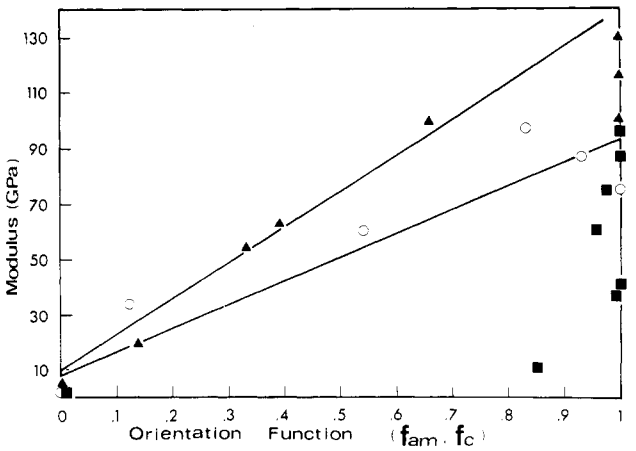

Figure 10. Dynamic (○) and sonic modulus (▲) versus amorphous orientation function f_{am} and dynamic modulus (■) versus crystalline orientation function f_c.

noted that the observed limiting modulus (100–120 GPa) is significantly lower than the values of the maximum attainable modulus (200–300 GPa) reported for polyethylene by other investigators.[28-30] This is probably related to the fact that no attempt was made to optimize the effectiveness of the drawing process in the present work. For example, it is known that the maximum attainable modulus depends on the draw temperature; in fact the modulus/draw temperature curve generally shows a maximum whose position compounds to the highest temperature at which effective drawing can take place.[31,32] Therefore, it is expected that the limiting value of the modulus in the modulus/draw ratio relation (Figure 9) would change with the draw temperature. Experiments along these lines are currently in progress.

It may also be noted that the two different methods of measuring the modulus give consistent but significantly different results. This may indicate that the two methods assess the contributions of the amorphous and crystalline phases in different ways.

It is of interest to ascertain whether the increase in modulus develops from the rearrangements in the crystalline or amorphous regions. For this purpose the modulus is plotted against the orientation functions f_c and f_{am}. It was found (Figure 10) that the modulus increases approximately linearly with the amorphous orientation function f_{am}, while there is no correlation with the crystalline orientation function f_c. Thus the increase in modulus in the extension range up to $\lambda = 100$ is principally due to changes in molecular orientation in the amorphous regions. A similar conclusion has been reached by Mirabella[33] in a study of highly drawn polypropylene films.

Conclusions

In the present work measurements of crystallinity, melting temperature, birefringence, crystalline and amorphous orientation, and tensile modulus have been made on dry gelation-crystallized films as a function of draw ratio. From the analysis of the data the following basic conclusions can be drawn. (1) All properties approach a limit at a draw ratio that corresponds approximately to the minimum draw ratio expected for full chain extension.[34] Further drawing apparently occurs by chain slippage. These results are consistent with recent theoretical predictions[35] on the development of the axial Young's modulus with draw ratio of flexible-chain polymers. (2) In the early stages of the drawing process the initial folded chain lamella structure is disrupted forming small-folded chain blocks (crystallites) that become rapidly reoriented with their c axes parallel to the draw direction. This process is accompanied by a decrease in crystallinity and melting temperature and is completed at a relatively low draw ratio ($\lambda \simeq 10$). Subsequently with increasing draw ratio trapped molecular entanglements and chain folds are removed during the transformation to a fibrous extended chain structure. (3) During the drawing process the molecules orient themselves more rapidly in the crystalline phase than in the amorphous phase. (4) The increase in modulus with draw ratio is not associated with the crystallite reorientation but with the rearrangements that occur in the amorphous phase, such as the decrease in the number of chain entanglements and the removal of the fold surfaces.

Acknowledgment. We thank Professors R. J. Samuels, R. S. Porter, and Paul Smith for helpful discussion and valuable suggestions. We also gratefully acknowledge the support of the Natural Science and Engineering Research Council of Canada and the Ministère de l'éducation du Quebec.

Registry No. Polyethylene, 9002-88-4.

References and Notes

(1) Smith, P.; Lemstra, P. J. *Colloid Polym. Sci.* **1980**, *258*, 7.
(2) Smith P.; Lemstra, P. J. *J. Polym. Sci, Polym. Phys. Ed.* **1981**, *19*, 1007.
(3) Barham, P. J.; Keller, A. *J. Mater. Sci.* **1985**, *20*, 2281.
(4) Wunderlich, B. *Macromolecular Physics*; Academic: New York, 1973.
(5) Samuels, R. J. *Structured Polymer Properties*; Wiley: New York, 1974.
(6) Samuels, R. J. *J. Polym. Sci., Polym. Phys. Ed.* **1965**, *3*, 1741.
(7) Read, B. E.; Stein, R. S. *Macromolecules* **1968**, *1*, 116.
(8) Onogi, S.; Asada, T. *Prog. Polym. Sci. Jpn.* **1971**, *2*, 261.
(9) Matsuo, M.; Manley, R. St. J. *Macromolecules* **1982**, *15*, 985. Ibid. *Macromolecules* **1983**, *16*, 1500.
(10) Adams, W. W.; Briber, R. M.; Sherman, E. S.; Porter, R. S.; Thomas, E. L. *Polymer* **1985**, *26*, 17.
(11) Wedgewood, A. R.; Seferis, J. C. *Polym. Eng. Sci.* **1984**, *24*, 328.
(12) Glenz, W.; Peterlin, A. *J. Macromol. Sci., Phys.* **1970**, *B4*(3), 473.
(13) Smook, J.; Pennings, A. J. *Colloid Polym. Sci.* **1984**, *262*, 712.
(14) Chuah, H. H.; DeMicheli, R. E.; Porter, R. S. *J. Polym. Sci., Polym. Lett. Ed.* **1983**, *21*, 791.
(15) Furuhata, K.; Yokokawa, T.; Miyasaka, K. *J. Polym. Sci., Polym. Phys. Ed.* **1984**, *22*, 133.
(16) Gopalan, M.; Mandelkern, L. *J. Phys. Chem.* **1967**, *71*, 3833.
(17) Pennings, A. J.; Zwijnenburg, A. *J. Polym. Sci., Polym. Phys. Ed.* **1979**, *17*, 1011.
(18) Clements, J.; Ward, I. M. *Polymer* **1982**, *23*, 935.
(19) Bunn, C. W.; de Daubeny, R. *Trans. Faraday Soc.* **1954**, *50*, 1173.
(20) Cannon, G. C. *Polymer* **1982**, *23*, 1123.
(21) Furuhata, K.; Yokokawa, T.; Seoul, C.; Miyasaka, K. *J. Polym. Sci., Polym. Phys. Ed.* **1986**, *24*, 59.
(22) Stein, R. S. *J. Polym. Sci.* **1959**, *34*, 709.
(23) Moy, F. H. Ph.D. Thesis, McGill University, Montreal, Canada, 1980.
(24) Nakayama, K.; Kanetsuna, H. *J. Mater. Sci.* **1975**, *10*, 1105.
(25) Mead, W. T.; Desper, C. R.; Porter, R. S. *J. Polym. Sci., Polym. Phys. Ed.* **1979**, *17*, 859.
(26) Roy, S. K. Ph.D. Thesis, McGill University, Montreal, Canada, 1986.
(27) Pezzutti, J. L.; Porter, R. S. *J. Appl. Polym. Sci.* **1985**, *30*, 4251.
(28) Sawatari, C.; Matsuo, M. *Colloid Polym. Sci.* **1985**, *263*, 783.
(29) Savitsky, A. V.; Gorshkova, I. A.; Frolova, I. L.; Shmikk, G. N.; Ioffe, A. F. *Polym. Bull. (Berlin)* **1984**, *12*, 195.
(30) Kanamoto, T.; Tsuruta, A.; Tanaka, K.; Takeda, M.; Porter, R. S. *Polymer J. (Tokyo)* **1983**, *15*, 327.
(31) Capaccio, G.; Gibson, A. G.; Ward, I. M. In *Ultra-High Modulus Polymers*; Ciferri, A., Ward, I. M., Eds.; Applied Science: London, 1979.
(32) Gogolewski, S.; Pennings, A. J. *Polymer* **1985**, *26*, 1394.
(33) Mirabella, F. M. *Polym. Mater. Sci. Eng.* **1985**, *53*, 751.
(34) Kanamoto, T.; Porter, R. S. *J. Polym. Sci., Polym. Lett. Ed.* **1983**, *21*, 1005.
(35) Irvine, P. A.; Smith P. *Macromolecules* **1986**, *19*, 240.